Density Functional Theory Calculations of Pressure Effects on the Vibrational Structure of α-RDX

M. S. Miao, Z. A. Dreger, J. M. Winey, and Y. M. Gupta*

Institute for Shock Physics and Department of Physics, Washington State University, Pullman, Washington 99164-2816

Received: August 14, 2008; Revised Manuscript Received: September 18, 2008

Pressure effects on the vibrational structure of α-RDX were examined using density functional theory (DFT) up to 4 GPa. The calculated vibrational frequencies at ambient conditions are in better agreement with experimental data than are previous single molecule calculations. The calculations showed the following pressure-induced changes: (i) larger shifts for lattice modes and for internal modes associated with the CH_2 and NO_2 groups as compared to the pressure shifts for modes associated with the triazine ring, (ii) enhancement of mixing between different vibrations, for example, between NN stretching and CH_2 scissor, wagging, twisting vibrations, and (iii) increase in mixing between translational lattice vibrations and the NO_2 wagging vibrations, reducing the distinction between internal and lattice modes. The calculated volume and lattice constants at ambient pressure are larger than the experimental values, due to the inability of the present density functional approach to correctly account for van der Waals forces. Consequently, the pressure-induced frequency shifts of many modes deviate substantially from experimental data for pressures below 1 GPa. With increasing pressure, both the lattice constants and the frequency shifts agree more closely with experimental values.

I. Introduction

Hexahydro-1,3,5-trinitro-*s*-triazine (RDX) is an important energetic crystal widely used as a secondary explosive and in propellants. A good understanding of the physical and chemical changes that occur in compressed RDX is needed for the development of a predictive capability regarding its sensitivity, performance, and safety under various conditions. To gain insight into these issues, knowledge of the molecular response under compression is required. As shown previously for PETN (Pentaerythritol tetranitrate)[1−4] and RDX,[5−8] progress in understanding microscopic processes in shocked energetic crystals can be achieved through a concerted experimental and computational approach. For example, changes in the molecular structure and intermolecular interactions can be probed efficiently with vibrational spectroscopies.[5,6] Here, we present density functional theory (DFT) calculations of the structural and vibrational properties of α-RDX under static compression to complement existing experimental data. Of particular interest are changes in the frequencies and atomic motions relevant to the vibrational modes.

It is known that RDX crystals can exist in three polymorphic phases, α-, *β*-, and *γ*-RDX.[9,10] Among these, α-RDX is stable for pressures below ∼4 GPa and for temperatures from 150 to 375 K. This polymorph has an orthorhombic structure with *Pbca* space group.[11] The molecules in the crystal assume the AAE conformation; that is, two NO_2 groups are in the axial position, while another NO_2 group is in the equatorial position. This molecular structure has approximate C_s symmetry with a slight deviation caused by the crystal field. The effect of pressure on the crystal and vibrational structure of α-RDX has been examined with X-ray diffraction[12,13] and with various spectroscopic methods, including Raman,[14−17] infrared (IR),[18] and inelastic neutron scattering (INS).[19] The X-ray diffraction measurements provided changes in the unit cell parameters, without any further information on the modification of the molecular and crystal structure. Spectroscopic experiments were primarily focused on the examination of polymorphic transformations.

Recently, the pressure dependence of the internal and lattice vibrational modes was examined by Dreger and Gupta,[5] who measured the Raman spectra of RDX single crystals under hydrostatic pressures up to 15 GPa. They found that pressure has a larger effect on lattice modes and on peripheral modes such as CH stretching and NO_2 torsion in comparison to the triazine ring modes. Furthermore, for RDX crystals under shock compression,[6] a large pressure dependence was observed for the CH stretching modes, consistent with the hydrostatic compression results.[5]

There have been several previous computational studies of molecular, crystal, and vibrational structures of RDX using quantum mechanical methods.[19−24] Rice and Chabalowski[20] calculated vibrational frequencies for various molecular conformers of RDX molecule. They indicated that both the Hartree−Fock method with MP2 correction and the density functional method with B3LYP hybrid functional accurately predicted molecular geometry in the gas phase. On the other hand, the calculated vibrational frequencies for a single molecule showed noticeable differences with the experimental values obtained for the crystal. Recently, Ciezak and Trevino[23] calculated the vibrational frequencies for α-RDX at ambient pressure and found better agreement with experimental spectra (Raman, IR, and INS) than were obtained from single molecule calculations.[20] However, the experimental lattice constants were used in those calculations.[23] The lattice constants were calculated by Byrd et al. at ambient conditions[22] and at high pressures up to 4 GPa.[24] They found that the calculated volume and lattice constants for α-RDX were significantly larger than the experimental values due to the inability of generalized gradient approximated (GGA) density functionals to account properly for van der Waals forces. However, improved agreement

* Corresponding author. E-mail: ymgupta@wsu.edu.

10.1021/jp807285u CCC: $40.75
Published on Web 10/31/2008

TABLE 1: Calculated and Experimental Volume and Lattice Constants at Ambient Pressure

	calc. (this work)	calc.[a]	exp.[b]	exp.[c]
V (Å^3)	1861.69	1884.5	1633.86	1641.45
a (Å)	13.65	13.69	13.182	13.20
b (Å)	11.84	11.93	11.574	11.60
c (Å)	11.51	11.54	10.709	10.72

[a] Reference 24. [b] Reference 12. [c] Reference 13.

between calculated and experimental values was observed at higher pressures.

In this work, we used density functional theory calculations to examine the effect of pressure on the vibrational structure and molecular geometry of α-RDX. The symmetry and the nature of the atomic displacements for both internal and lattice modes were assigned. For the first time, the pressure shifts of the vibrational frequencies were calculated and compared to Raman measurements. We also examined how the inability to account for van der Waals forces affects the calculations of vibrational spectra and their dependence on external pressures.

The rest of this Article is organized as follows. The computational methods and parameters are described in section II. The molecular, crystal, and vibrational structures of α-RDX at ambient conditions are presented in section III. In section IV, we present and discuss the effect of pressure. Finally, the main findings of the work are summarized in section V.

II. Computational Methods

Density functional theory[25] with the Perdew−Wang 91 (PW91)[26] GGA exchange-correlation functional was used as implemented in the Vienna Ab Initio Package (VASP).[27] Vanderbilt ultrasoft pseudopotentials[28] were applied to describe the ion core potentials. We tested the convergence of total energy, forces, and stresses with respect to the cutoff energy and k mesh and found that a cutoff energy of 550 eV and Γ point calculations give well-converged results for the geometry and vibrational frequencies. As shown by Byrd et al.,[22,24] the ultrasoft pseudopotential provides similar results as compared to the projector augmented wave (PAW) potential for the same cutoff energies.

The vibrational modes were calculated using the finite displacement method in which the atomic forces and dynamical matrix are computed for small displacements of the atoms from the equilibrium structure. The magnitude of the displacements (0.01 Å) was selected as a compromise based on two competing needs: the displacements should be small enough to provide accurate derivatives, while being large enough so that calculated energy changes are large as compared to the numerical errors in the calculations. To reduce the computation time, the minimum number of displacements was used, and the reduced dynamical matrix was constructed according to the symmetry of the crystal. A phonon calculation program[29] was utilized to calculate the vibrational modes from the symmetry-reduced dynamical matrix.

The symmetry and atomic motions of each vibrational mode were assigned by separating and visualizing the motions of the RDX molecule (for internal modes), as well as the motions of the center of the mass of the molecules in a unit cell (for lattice modes). The visualization was performed with the Molden-4.4 software.

III. Ambient Pressure

Crystal and Molecular Structure. As shown in Table 1, we obtained a unit cell volume of 1861.69 Å^3, which is 14% larger than the experimental value[12] of 1641 Å^3. Our value is close to the recently calculated value of 1884.5 Å^3 obtained from the density functional calculation[22,24] using ultrasoft pseudopotentials and the PW91 GGA functional. The kinetic energy cutoff of that calculation was 545 eV, which is close to our cutoff energy. As pointed out in ref 22, the large discrepancy between calculated and experimental values results from the lack of the van der Waals forces in the GGA functional. We also confirmed that a large basis set is necessary to obtain a converged volume. In the case of α-RDX, a smaller kinetic energy cutoff of 400 eV results in a volume much closer to the experimental value because of erroneous binding forces resulting from an insufficient basis set.

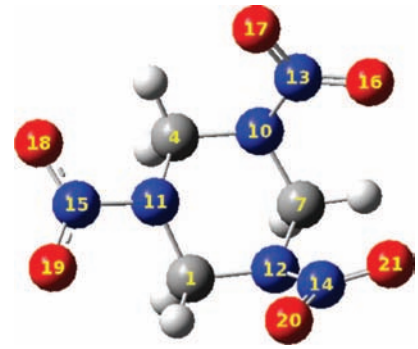

Figure 1. Geometry of the RDX molecule in the α-polymorph. Carbon atoms are in gray, nitrogen atoms in blue, oxygen atoms in red, and hydrogen atoms in white.

As shown in Table 1, the calculated lattice constants a, b, and c are 13.65, 11.84, and 11.51 Å, which are 3.5%, 2.3%, and 7.5% larger than the experimental values. The anisotropy is likely caused by differences in the intermolecular interactions along different directions. The interactions between the H atoms on the triazine rings and the nitro groups on the neighboring RDX molecules can result in stronger interactions in the a and b directions. Such interactions are described more accurately by DFT and result in better values for a and b as compared to c.

Our calculations also showed that the deviation from C_s symmetry for the RDX molecule is quite small under ambient pressure. For example, the bond lengths of C7−N10 and C7−N12 (see Figure 1), which are equivalent in C_s symmetry, are almost identical. The breaking of C_s symmetry appears more obvious for C−N−N angles, which are the measurements of the bend angles of nitro groups with respect to the triazine ring. The angle C4−N12−N14 is 133°, whereas the equivalent angle in C_s symmetry, C1−N10−N13, is 127°.

Internal Vibrational Modes. Table 2 lists the characteristics of the calculated internal vibrational modes for the α-RDX polymorph,[30] including frequencies, symmetry assignments, and shifts of the frequencies under pressure. The pressure shifts are discussed in section IV. Table 2 also compares the calculated frequencies to previous single molecule calculations[20] and to Raman spectroscopy data,[5,14] and describes the atomic motions associated with the vibrations. Because there are 21 atoms in each RDX molecule, there are a total of 57 internal modes. As can be seen in Table 2, the modes with different vibrations such as CH_2 stretching, ONO stretching, CN stretching, etc., are grouped and well separated. However, the NN stretching vibrations strongly mix with the CH_2 scissor, wagging, and twisting vibrations. Furthermore, the CH_2 rocking, the ONO scissor, and the NO_2 rocking vibrations mix with the triazine ring vibrations.

The frequencies obtained in our calculations generally agree better with experimental values than the frequencies obtained

TABLE 2: Characteristics of Internal Vibrational Modes of α-RDX under Ambient Pressure and the Pressure Dependencies of Frequencies[a]

	frequency (cm^{-1})				vibration assignment[e]	molecular symmetry		dν/dp		
	this work (PW91 GGA)	exp.[b]	exp.[c]	calc.[d] (B3LYP/ 6-311+G**)	this work	this work	calc.[d]	this work[f]		exp.[b,g]
1	3141	3076 (ν_1)	3075	3206	CH st (eq; C7)	A′	A′	1.3	−2.0	2.3
2	3136	3067 (ν_2)	3067	3199	CH st (eq, C1+C4)	A′	A′	4.7	4.0	7.1
3	3125			3205	CH st (eq, C4+C1)	A″	A″	4.2	4.6	
4	3043	3003 (ν_3)	3001	3081	CH st (ax, C7)	A′	A′	10.5	5.9	8.6
5	2998	2949 (ν_4)	2949	3016	CH st (ax, C1+C4)	A′	A′	6.3	3.5	10.2
6	2984	2906 (ν_5)		3015	CH st (ax, C4+C1)	A″	A″	8.7	7.6	5.1
7	1601	1595 (ν_7)	1593	1668	O−N−O st (N13+N14)	A′	A′	4.7	3.4	0.8
8	1580	1573 (ν_8)	1570	1648	O−N−O st (N13+N14)	A″	A″	2.1	2.1	1.7
9	1551	1542 (ν_9)	1538	1623	O−N−O st. (N15)	A″	A″	−3.1	−0.8	0.2
10	1448	1508 (ν_{12})	1508	1496	N−N st (N11−N15) + CH_2 sci (C1+C4)	A′	A′	−2.5	1.9	2.0
11	1422	1460 (ν_{14})	1456	1480	N−N st (all) + CH_2 sci (all)	A′	A″	−2.5	0.3	1.7
12	1409	1436 (ν_{15})	1433	1468	CH_2 sci (C1+C4)	A″	A′	−2.9	1.0	1.1
13	1385	1422 (ν_{17})	1422	1420	N−N st (N11−N15) + CH_2 sci (C7)	A′	A′	−2.5	2.6	0.6
14	1353	1388 (ν_{18})	1387	1406	N−N st (N10−N13+N12−N14) + CH_2 wag (all)	A″	A″	1.8	1.6	2.8
15	1335	1377 (ν_{19})	1377	1374	N−N st (all) + CH_2 wag (C1 +C4)	A′	A″	4.0	4.9	1.9
16	1322	1351 (ν_{21})	1346	1362	CH_2 tw (C7) + CNC st (N10+N12)	A″	A″	2.6	1.7	4.3
17	1312	1309 (ν_{23})	1309	1362	CH_2 tw (C1+C4) +N−N st(N10−N13+N12−N14)	A′	A′	2.5	2.6	4.9
18	1306			1299	CH_2 wag (all) + ring tw {rot}	A″	A″	0.7	1.4	
19	1287	1273 (ν_{24})	1273	1337	CH_2 wag (C1+C4) + N−N st (all)	A′	A′	3.5	4.3	1.6
20	1255	1273 (ν'_{24})		1270	CH_2 wag (C7) +N−N st (N10−N13+N12−N14)	A″	A″	3.3	4.1	4.1
21	1222	1249 (ν_{25})		1296	CNC st (N11+N12)	A′	A′	2.6	4.3	5.1
22	1226	1249 (ν_{25})		1264	CNC st (N10+N12)	A′	A′	2.9	3.0	
23	1215	1232 (ν_{26})	1232	1238	CNC st (all) + CH_2 tw (all)	A″	A″	3.3	2.6	3.7
24	1210	1215 (ν_{27})	1214	1230	CNC st (all)+ N−N st (all)	A′	A′	2.8	3.9	3.2
25	1112	1031 (ν_{28})	1029	1153	ring {Kekule}	A″	A″	3.9	4.0	8.5; 6.9
26	1058	1023 (ν_{29})		1036	CNC st (N11) + N−N st (N11−N15) + ONO st (N15)	A′	A″	−6.1	5.2	3.7
27	997	945 (ν_{30})	943	1011	CH_2 r (C1+C4) + CN st (C1−N12+C4−N10) + N−N st (N10−N13+N12−N14)	A″	A′	3.7	3.8	6.0
28	935	920 (ν_{31})	920	951	CH_2 r (C1+C4) + ring b + N−N st (all)	A′	A′	4.0	4.5	3.8
29	916	885 (ν_{32})	884	937	CH_2 r (C7) + CN st (C1−N12+C4−N10) + N−N st (N10−N13+N12−N14)	A′	A″	0.0	2.1	2.7
30	886	858 (ν_{33})	855	909	CN st (C7−N12+C7−N10) + N−N st (N10−N13+N12−N14)	A″	A″	4.3	4.9	2.8
31	868	848 (ν_{34})	847	896	ring CNC st (N10+N12) + NO_2 sci (N13 + N14)	A′	A′	1.7	3.4	4.3
32	835			870	ring CNC st (N10+N12) + NO_2 sci (N13 + N14)	A″	A″	3.9	4.5	
33	827	788 (ν_{35})	786	855	ring CNC st (N11) + NO_2 sci (N15)	A′	A′	2.3	2.8	2.4
34	760	757 (ν_{36})	756	803	ring NCN sci (all) + NO_2 sci (all)	A′	A′	2.3	3.1	0.4
35	725	739 (ν_{37})	739	769	NNO_2 u (N13+N15)	A′	A′	0.7	1.5	1.5
36	721			761	NNO_2 u (N13+N14)	A″	A″	0.1	1.2	
37	711			756	NNO_2 u (N14+N15)	A′	A′	−1.4	−2.2	
38	659	670 (ν_{38})	669	676	ring b + NO_2 sci (all)	A′	A′	2.7	1.5	5.1; 3.3
39	635	607 (ν_{39})	605	651	ring tw + NO_2 sci (N13+N14)	A″	A″	4.4	5.4	5.4
40	593	590 (ν_{40})	589	610	ring tw + NO_2 r (N13+N14)	A′	A′	4.7	4.3	7.1; 6.4
41	583	588 (ν_{41})		588	ring tw {rot} + NO_2 r (all)	A″	A″	5.3	4.8	5.7; 4.8
42	577	488 (ν_{42})	486	579	ring tw {along C1−N10} + NO_2 r (all)	A″	A′	4.3	3.4	6.2
43	455	464 (ν_{43})	463	463	ring b {folding}	A′	A′	10.4	9.0	5.8; 0.0
44	416	429 (ν_{44})		438	ring b {fattening}	A′	A′	6.3	3.8	3.3; 0.3
45	399	415 (ν_{45})		403	NNC_2 u (N10+N12)	A″	A″	8.5	7.4	3.8
46	393	364 (ν_{46})	414	406	NNC_2 u (N11) + NO_2 r (N13+N14)	A′	A′	6.3	4.4	6.4; 3.4
47	355	347 (ν_{47})	347	371	ring tw	A″	A″	4.3	4.5	4.9
48	338	301 (ν_{48})		325	ring st {C7−N11 direction}	A′	A′	4.0	0.2	7.1
49	302	226 (ν_{49})	224	290	ring tw {rot} NO_2 r (all)	A″	A″	5.0	1.2	6.4
50	226	207 (ν_{50})	205	209	N−NC_2 u (N11+N10) + NO_2 r (N14)	A″	A″	6.1	1.7	6.7
51	217			229	N−NC_2 u (N11+N12) + NO_2 r (N13)	A′	A′	5.4	4.2	
52	178	149 (ν_{51})		107	NO_2 rot (N15+N14)	A″	A′	8.1	7.4	18.7; 2.7
53	171	131 (ν_{52})		93	NO_2 rot (N14)	A′	A″	4.7	7.7	21; 5.4
54	158			74	NO_2 rot (N13)	A″	A″	2.0	2.1	
55	144	107 (ν_{53})	106	63	NO_2 wag (N14) + lattice	A″	A′	2.8	1.1	16.7; 8.7
56	123			60	NO_2 wag (N15) + lattice	A″	A′	7.4	5.2	
57	116	90 (ν_{54})	90	44	NO_2 wag (N13+N14) + lattice	A′	A″	6.9	10.4	17.7; 3.3

[a] The blank lines separate the modes into groups with different natures of atomic motions. The frequencies from this work as well as from ref 20 were not scaled. [b] Reference 5. [c] Reference 14. [d] Reference 20. [e] Abbreviations: st = stretch, eq = equatorial, ax = axial, tw = twist, sci = scissor, r = rock, b = bend, u = umbrella, rot = rotation, wag = wagging, tor = torsion. Parenthesized notations defined the locations of the vibrations; bracketed notations further describe the vibrations. Notations in parentheses are the same as in Table 1 in ref 5. [f] The values in the lefthand column were calculated using frequencies at ambient pressure and 3 GPa; the values in the righthand column were calculated using frequencies at 1 and 3 GPa. [g] The second experimental value of dν/dp was calculated at 3.8 GPa.

previously from single molecule calculations.[20] This is most likely due to the inclusion of crystal field effects in our calculations. The observed discrepancies between our calculations and the experimental values depend on the nature of the mode. For example, the CH stretching frequencies are considerably higher than the values observed in the Raman measurements, and the ONO stretching frequencies are lower. It should be noted that Ciezak and Trevino[23] obtained better agreement with the experimental values; however, they used the experimental lattice parameters in their calculations.

TABLE 3: Frequencies of Lattice Modes of α-RDX and Their Pressure Dependencies[f]

modes	sym	freq this work	freq exp.[a]	freq exp.[b,c]	dν/dp this work[d]		dν/dp exp.[b,c]
Trans3 (L_6)	A_g	98	70	69, 72, 76	7.2	8.0	12.3, 14.0, 16.3
	B_{1g}	91	70				
	B_{2g}	98	74				
	B_{3g}	100	70				
Trans2 (L_5)	A_g	88	59	60	8.9	8.6	11.2
	B_{1g}	80	59				
	B_{2g}	85	60				
	B_{3g}	77	59				
Trans1 (L_4)	A_g	73	51	46, 51	9.0	11.4	12.7, 11.7
	B_{1g}	68	52				
	B_{2g}	74	49				
	B_{3g}	66	49				
Libr3 (L_3)	A_g	60	51		9.8	11.6	
	B_{1g}	56	46				
	B_{2g}	54	−				
	B_{3g}	53	49				
Libr2 (L_2)	A_g	52	33	29, 38	8.2	16.8	4.6, 5.3
	B_{1g}	48	28				
	B_{2g}	28	29				
	B_{3g}	41	37				
Libr1 (L_1)	A_g	32	20	21	5.0	9.0	2.8
	B_{1g}	−38[e]	20				
	B_{2g}	−30[e]	20				
	B_{3g}	−25[e]	19				

[a] Reference 15. [b] Reference 5. [c] Different values correspond to different observed Raman peaks with unknown symmetry assignments. [d] The values in the lefthand column were calculated using frequencies at ambient pressure and 3 GPa; the values in the righthand column were calculated using frequencies at 1 and 3 GPa. [e] The three Libr1 modes that resulted in negative frequencies were not used in calculating the pressure shifts for the Libr1 (L1) mode. [f] The calculated frequencies from this work were not scaled.

Lattice Modes. Because there are eight RDX molecules in the unit cell, the total number of lattice modes is 42. Among them, 24 are of even parity to the inversion symmetry of D_{2h} point group. These modes are Raman active and were resolved by previous polarized Raman experiments.[15,16] In Table 3, the calculated frequencies, symmetry assignments, and pressure dependence of the Raman active lattice modes of α-RDX are compared to the experimental data. The lattice mode frequencies are all below 100 cm^{-1}, and the calculated frequencies are generally 10−30 cm^{-1} higher than the experimental values. Examination of the atomic motions reveals that the translational lattice vibrations mix somewhat with the NO_2 wagging vibrations. However, the modes are distinctively dominated by lattice vibrations, indicating the existence of a clear boundary between internal and lattice modes.

IV. Hydrostatic Pressure

Crystal and Molecular Structure. In Figure 2, we present the calculated volume and lattice constants of α-RDX under hydrostatic pressure up to 4 GPa. These results are compared to the previous calculations[24] and experimental data.[12] Consistent with the previous calculations, our calculated volume and lattice constants agree more closely with the experimental data with increasing pressure. At 4 GPa, the calculated volume is only about 5% larger than the experimental value; and the calculated lattice constants *a*, *b*, and *c* are about 1.7%, 1.2%, and 2.5% larger. The reductions of volume and lattice constants *a*, *b*, and *c* at 4 GPa are 22%, 5.6%, 7.3%, and 10.9% in our calculations. The reduction is the largest along the *c* direction due to weaker intermolecular interactions along this direction.

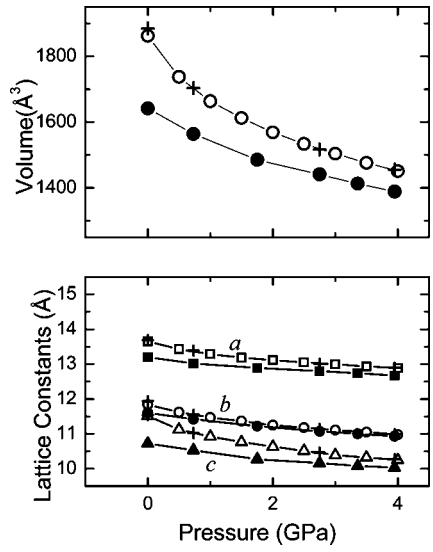

Figure 2. Pressure-induced changes in volume and lattice constants for α-RDX. The open symbols show the current calculation results, and the solid symbols show the experimental results. The plus signs show the results of previous calculations.[24] The squares, circles, and the triangles in the lower panel are for the lattice parameters *a*, *b*, and *c*, respectively.

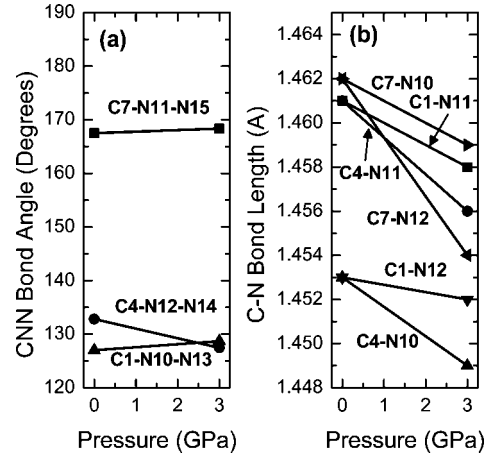

Figure 3. Effect of pressure on the geometry parameters of RDX molecules in the α polymorph: (a) CNN angles, (b) C−N bond lengths.

In contrast to the large volume reduction, changes in the molecular geometry under high pressure are relatively small. The largest change of bond length happens for the N−N bonds between the N atoms in the triazine ring and the N atoms in the NO_2 side groups. The three N−N bond lengths change by 1.1%, 0.6%, and 2.8% from ambient pressure to 3 GPa. The changes in the other bond lengths and angles were generally smaller than 0.5%. As shown in Figure 3a, the three C−N−N angles change only slightly with pressure, indicating that the RDX molecules remain in the AAE conformation. On the other hand, pressure causes a considerable deviation from the approximate C_s molecular symmetry. As shown in Figure 3b, the bond lengths of equivalent C−N bonds under C_s symmetry are identical at ambient pressure but are substantially different under hydrostatic pressure. Only the values at ambient pressure and 3 GPa are presented in Figure 3, because the changes of molecular geometry are small for intermediate pressures and are, therefore, considerably influenced by numerical fluctuations. The data presented above can be useful in understanding the molecular mechanisms leading to the phase transition observed at ∼4 GPa.[9,10]

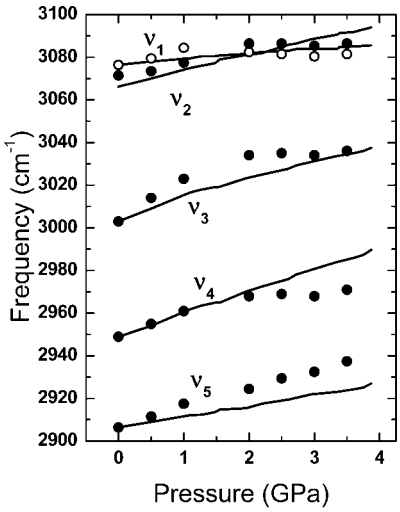

Figure 4. Frequency shift for C−H stretching modes under pressure. The symbols represent the calculated results. The solid lines are experimental data.[5] The calculated frequencies at all pressures are shifted by the same amount so that the calculated values and the experimental values match at ambient pressure, except for ν_1 and ν_2, which are shifted by equal amounts. To distinguish between modes that are close in frequency, the mode ν_1 is denoted by ○.

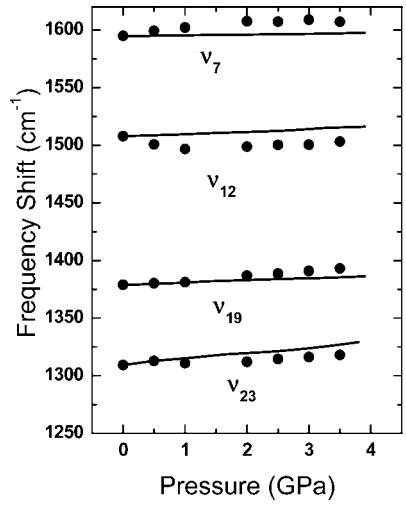

Figure 5. Frequency shift for N−N and N−O stretching modes under pressure. The symbols represent the calculated results. The solid lines are experimental data.[5] The calculated frequencies at all pressures are shifted by the same amount so that the calculated values and the experimental values match at ambient pressure.

Internal Vibrational Modes. The Raman spectroscopy data for RDX under hydrostatic pressure showed that most of the frequencies of the internal modes shift quite linearly with increasing pressure.[5] Therefore, the first-order derivatives of frequencies with respect to pressure were used to characterize the pressure dependence of frequency. We calculated these derivatives numerically using the frequencies at ambient pressure and at 3 GPa. The derivatives were also calculated using frequencies at 1 and 3 GPa to examine the pressure dependence of the frequencies over different pressure ranges. The results are listed in Table 2 and are compared to the corresponding values from Raman spectroscopy.[5] As can be seen, pressure derivatives calculated using frequencies in the range from 1 to 3 GPa show better overall agreement with the experimental values as compared to those calculated using frequencies from ambient pressure to 3 GPa. This result shows the effect of the inadequate treatment of van der Waals interactions in DFT calculations at lower pressures. However, as shown below, this deficiency in DFT calculations affects some vibrational modes more significantly than others.

Figure 4 shows the calculated vibrational frequencies for the CH stretching modes together with the experimental results.[5] To facilitate comparison of the pressure dependence, the calculated frequencies at all pressures are shifted by the same amount so that the calculated values and the experimental values match at ambient pressure. The modes with the highest frequencies are the stretching modes of the three equatorial C−H bonds. As shown in Table 2, the frequencies of these three modes are very close to each other, only 5−10 cm^{-1} apart. The two A′ modes were observed in the Raman study and are shown in Table 2 and Figure 4. In previous Raman experiments,[5] these two modes are interpreted as crossing in frequency under compression. Here, we confirm this crossing by examination of the calculated atomic motions in each vibrational mode. At ambient pressure, the atomic motions of the ν_1 mode localize on C7−H bond, which is the equatorial C−H bond between the two axial NO_2 groups (see Figure 1). On the other hand, the ν_2 mode is the symmetric combination of vibrations of C1−H and C4−H bonds. Our calculations, at 3.5 GPa, show clearly that the C7−H stretching mode becomes lower in frequency than the mode corresponding to the combinative vibrations of C1−H and C4−H bonds, indicating a crossing under pressure.

The other three CH stretching modes, located between 2900 and 3040 cm^{-1}, are the modes of the axial C−H bonds. They are well separated from each other and from the stretching modes of the equatorial C−H bonds, indicating that the C−H bonds and their interactions with the neighboring RDX molecules are quite different for the axial and equatorial H atoms. Figure 4 shows that the stretching modes of axial C−H bonds have larger pressure dependence than the stretching modes of the equatorial C−H bonds.

The NO stretching modes of the nitro groups are clustered in the frequency range from 1550 to 1600 cm^{-1}. These modes are separated by 20−30 cm^{-1}. The highest frequency is for the symmetric stretching vibration of the nitro groups at the two axial sites and the second highest for the antisymmetric stretching vibration. NO stretching at the equatorial site has the lowest frequency. The pressure dependence of the experimental and calculated frequencies of the symmetric stretching modes of axial NO_2 is shown in Figure 5. It is clear that the agreement between calculated and experimental shifts varies with pressure. At pressures below 1 GPa, the calculated and experimental shifts are quite different. However, for pressures larger than 1 GPa, the calculated frequency shifts almost parallel the experimental data. The large pressure dependence of the CH_2 and NO_2 stretching modes is consistent with their location on the periphery of the molecule and is in agreement with experimental results.[5]

The NN stretching modes have frequencies lower than the NO stretching modes. An important feature of these modes is that they mix strongly with the CH_2 scissor, wagging, and twisting vibrations. Figure 5 presents the pressure dependence of selected NN stretching modes that occur in combination with CH_2 scissor (ν_{12}), wagging (ν_{19}), and twisting (ν_{23}) vibrations. Similar to NO stretching modes, the calculated frequency shifts show discrepancies as compared to experimental shifts below 1 GPa. It can be seen that the calculated frequency shift of NN stretching plus CH_2 scissor mode (ν_{12}) has a large negative slope below 1 GPa. As a result, the overall frequency shift from ambient pressure to 3 GPa is negative as shown in Table 2.

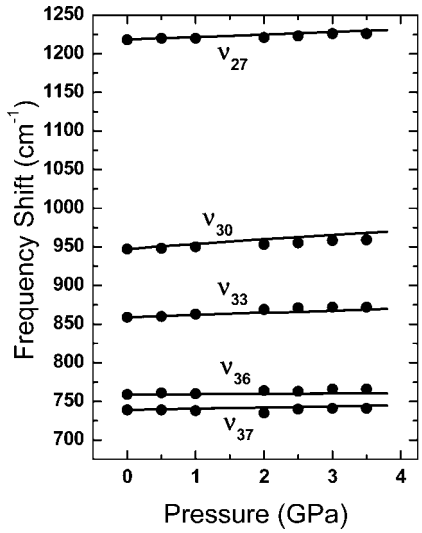

Figure 6. Frequency shift for C−N stretching modes under pressure. The symbols represent the calculated results. The solid lines are experimental data.[5] The calculated frequencies at all pressures are shifted by the same amount so that the calculated values and the experimental values match at ambient pressure.

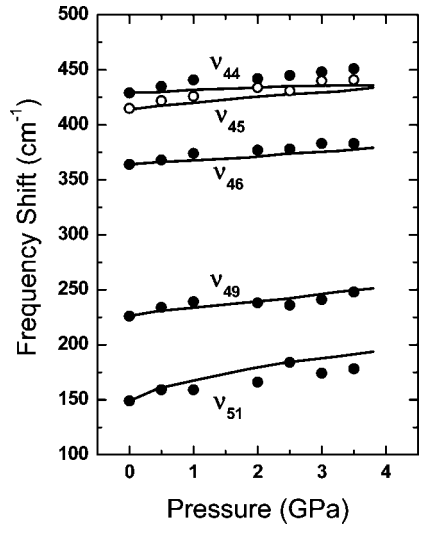

Figure 7. Frequency shift for the triazine ring modes under pressure. The symbols represent the calculated results. The solid lines are experimental data.[5] The calculated frequencies at all pressures are shifted by the same amount so that the calculated values and the experimental values match at ambient pressure. To distinguish between modes that are close in frequency, the mode ν_{45} is denoted by ○.

However, all of the NN stretching plus CH_2 scissor modes show positive slopes when calculated from 1 to 3 GPa.

The NN stretching modes correspond to important vibrational channels for the initial decomposition reactions.[31−35] The two major initial reactions for RDX decomposition are N−N homolysis[31,35] and HONO elimination.[33,34] In the former reaction, the N−N bond breaks, producing a NO_2 radical and an N-centered radical. In the latter reaction, a HONO molecule is eliminated from RDX, leaving behind a molecule with a *C*═N double bond on the triazine ring. Recently, we proposed[8] a concerted N−N homolysis and H migration reaction that generates an NO_2 radical and a C-centered radical to explain spectral features observed in the time-resolved emission spectroscopy data[7] for shocked RDX crystals. The strong mixing between the NN stretching vibrations and the CH_2 wagging and twisting vibrations provides potential vibrational channels for the above reaction.

Figure 6 shows the frequency shifts of representative vibrations in the range from 750 to 1250 cm^{-1}, including the CNC stretching (ν_{27}, ν_{33}), the CH_2 rocking (ν_{30}), the NCN scissor (ν_{36}), and the NNO_2 umbrella (ν_{36}) modes. These modes are well separated in frequency from the other modes and mix only slightly with other vibrations. The calculated pressure dependencies of these modes are found to be in good agreement with the Raman spectra as shown by Figure 6, even at pressures lower than 1 GPa. However, the modes in this frequency range are quite insensitive to pressure. These features can be attributed to the fact that the C−N bonds are on the triazine ring and are not significantly affected by interactions with neighboring molecules.

The ring modes, including twisting and breathing modes, are collective vibrations of all of the CN bonds on the triazine ring. Figure 7 shows the pressure dependence of representative ring modes (breathing ν_{44} and twisting ν_{49}) together with the NNC_2 umbrella (ν_{45} and ν_{46}) and the NO_2 rotational (ν_{51}) modes. The frequency shifts of these modes are relatively large. The calculations captured the general trend of the frequency shifts of these modes for both low (<1 GPa) and high pressure range (>1 GPa). For the modes with lower frequencies, the numerical errors in the calculation become significant, as shown in Figure 7. The ring mode is related to another important initial decomposition reaction, the concerted triple ring fission that produces three methylenenitramine (CH_2NNO_2) fragments.[36,37]

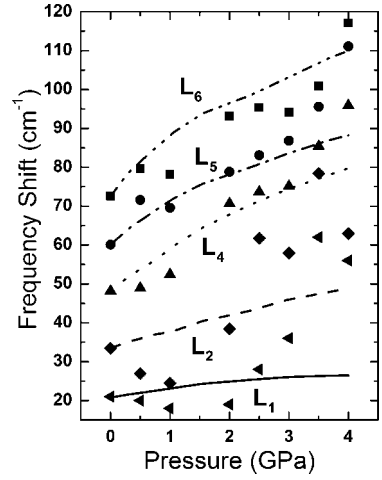

Figure 8. Frequency shift for lattice modes under pressure. The symbols represent the calculated results. The solid lines are experimental data.[5] The calculated frequencies at all pressures are shifted by the same amount so that the calculated values and the experimental values match at ambient pressure.

Lattice Modes. The 48 lattice modes form six groups, including three librational and three translational modes. As shown in Table 3, each group of lattice modes contains four Raman active modes with symmetry assignment of A_g, B_{1g}, B_{2g}, and B_{3g}. The recent Raman measurements under pressure[5] were not able to resolve all of the modes. For example, translational mode L_6 was resolved into three modes. However, it is not possible to assign the symmetry of each mode from the nonpolarized Raman spectra.[5] Therefore, we cannot compare the frequency shift for each individual mode. In Figure 8, we show the average value of the modes within each group for both theoretical and experimental results. The top three lines and symbols are the translational modes, and the lower two are the librational modes. One of the librational modes, L_3, is absent in the experimental Raman spectra, and therefore the corresponding calculated mode is not shown in Figure 8.

Although the uncertainty caused by numerical errors is significant for low energy modes, the calculated frequency shifts of the translational modes agree reasonably well with the Raman measurements[5,15] (at 4 GPa, the calculated frequencies for the L_6, L_5, and L_4 modes differ from the experimental values by 28%, 51%, and 48%, respectively). In contrast to the translational modes, the calculations for the librational modes showed large discrepancies in comparison with the experimental results (at 4 GPa, the calculated frequencies for the L_1 and L_2 modes differ from the experimental values by 154% and 47%, respectively). At pressures below 1 GPa, the calculated frequencies of librational modes have negative shifts with increasing pressure (see Figure 8). For pressures larger than 1 GPa, the calculated frequencies increase faster than the experimental frequencies. These results indicate that the current approach is not sufficiently accurate to calculate extremely low frequency lattice modes.

Last, pressure can also enhance the mixing between internal and lattice vibrations. As discussed in the previous section, the lattice translational modes mix with the NO_2 wagging modes at ambient pressure. Under high pressure, this mixing becomes stronger, and the distinction between internal and lattice modes tends to disappear. The lattice modes have large components of NO_2 wagging vibrations, and the NO_2 rotational and wagging modes show large lattice translational vibrations.

V. Summary and Conclusions

Density functional theory calculations were applied to examine the effect of pressure on the vibrational spectra and molecular geometry of α-RDX. The molecular geometry parameters are in good agreement with experimental results at ambient conditions. The vibrational frequencies at ambient pressure are in better agreement with experimental values than were earlier single molecule calculations. Despite the inability of GGA-DFT calculations to correctly account for van der Waals forces, the calculated frequency shifts under pressure are in good agreement with Raman measurements above 1 GPa. Below 1 GPa, the calculated shifts showed significant discrepancies with the experimental data, with some modes more affected than others. In addition, calculations for the low energy modes are substantially affected by numerical errors. Despite these two sources of inaccuracy, calculated lattice mode frequencies are in reasonable agreement with the experimental results.

Our calculations revealed the following pressure effects on the molecular geometry and the vibrational modes of α-RDX: (i) Hydrostatic pressure changes the molecular geometry only slightly. The RDX molecule remains in the AAE conformation but deviates considerably from C_s symmetry. (ii) Pressure has a stronger effect on the vibrational modes that are associated with the motions of the peripheral groups, that is, CH_2 and NO_2 side groups, in agreement with previous experimental results.[5] (iii) The mixing between different vibrations becomes stronger under pressure, including the mixing between NN stretching and CH_2 wagging, scissor, and twisting vibrations. The strong mixing between these vibrations provides potential vibrational channels for a proposed concerted N−N homolysis and H migration reaction reaction.[8] (iv) Consistent with previous experimental findings,[5] mixing between internal NO_2 wagging vibrations and lattice translational vibrations becomes stronger under pressure, reducing the distinction between internal and lattice modes.

Acknowledgment. We thank Drs. Warren Perger and James E. Patterson for valuable discussions. This work was supported by ONR MURI Grants N00014-01-1-0802 and N00014-06-1-0459, and DOE Grant DEFG0397SF21388.

References and Notes

(1) Gruzdkov, Y. A.; Gupta, Y. M. *J. Phys. Chem. A* **2000**, *104*, 11169.
(2) Dreger, Z. A.; Gruzdkov, Y. A.; Gupta, Y. M.; Dick, J. J. *J. Phys. Chem. B* **2002**, *106*, 247.
(3) Gruzdkov, Y. A.; Dreger, Z. A.; Gupta, Y. M. *J. Phys. Chem. A* **2004**, *108*, 6216.
(4) Hemmi, N.; Dreger, Z. A.; Gruzdkov, Y. A.; Winey, J. M.; Gupta, Y. M. *J. Phys. Chem. B* **2006**, *110*, 20948.
(5) Dreger, Z. A.; Gupta, Y. M. *J. Phys. Chem. B* **2007**, *111*, 3893.
(6) Patterson, J. E.; Dreger, Z. A.; Gupta, Y. M. *J. Phys. Chem. B* **2007**, *111*, 10897.
(7) Patterson, J. E.; Dreger, Z. A.; Miao, M. S.; Gupta, Y. M. *J. Phys. Chem. A* **2008**, *112*, 7374.
(8) Miao, M. S.; Dreger, Z. A.; Patterson, J. E.; Gupta, Y. M. *J. Phys. Chem. A* **2008**, *112*, 7383.
(9) Baer, B. J.; Oxley, J.; Nicol, M. *High-Pressure Res.* **1990**, *2*, 99.
(10) Miller, P. J.; Block, S.; Piermarini, G. J. *Combust. Flame* **1991**, *83*, 174.
(11) Choi, C. S.; Prince, E. *Acta Crystallogr., Sect. B* **1972**, *28*, 2857.
(12) Olinger, B.; Roof, B.; Cady, H. *Proceedings of International Symposium on High Dynamic Pressures*; Paris, France, 1978; p 3.
(13) Yoo, C. S.; Cynn, H.; Howard, W. M.; Holmes, N. C. *Proc. 11th Det. Symp.* **1998**, 951.
(14) Rey-Lafon, M.; Trinquecoste, C.; Cavagnat, R.; Forel, M. T. *J. Chim. Phys. Phys.-Chim. Biol.* **1971**, *68*, 1533.
(15) Rey-Lafon, M.; Cavagnat, R.; Trinquecoste, C.; Forel, M. T. *J. Chim. Phys. Phys.-Chim. Biol.* **1971**, *68*, 1575.
(16) Haycraft, J. J.; Stevens, L. L.; Eckhardt, C. J. *J. Appl. Phys.* **2006**, *100*, 053508.
(17) Ciezak, J. A.; Jenkins, T. A.; Liu, Z.; Hemley, R. J. *J. Phys. Chem. A* **2007**, *111*, 59.
(18) Karpowicz, R. J.; Brill, T. B. *J. Phys. Chem.* **1984**, *88*, 348.
(19) Harris, N. J.; Lammertsma, K. *J. Am. Chem. Soc.* **1997**, *119*, 6583.
(20) Rice, M. B.; Chabalowski, C. F. *J. Phys. Chem. A* **1997**, *101*, 8720.
(21) Vladimiroff, T.; Rice, B. M. *J. Phys. Chem. A* **2002**, *106*, 10437.
(22) Byrd, E. F. C.; Scuseria, G. E.; Chabalowski, C. F. *J. Phys. Chem. B* **2004**, *108*, 13100.
(23) Ciezak, J. A.; Trevino, S. F. *J. Phys. Chem. A* **2006**, *110*, 5149.
(24) Byrd, E. F. C.; Rice, B. M. *J. Phys. Chem. C* **2007**, *111*, 2787.
(25) (a) Hohenberg, P.; Kohn, W. *Phys. Rev. B* **1964**, *136*, 864. (b) Kohn, W.; Sham, L. J. *Phys. Rev. A* **1965**, *140*, 113.
(26) Burke, K.; Perdew, J. P.; Wang, Y. In *Electronic Density Functional Theory: Recent Progress and New Directions*; Dobson, J. F.; Vignale, G.; Das, M. P., Eds.; Plenum: New York, 1998.
(27) (a) Kresse, G.; Furthmüller, J.; Hafner, J. *Europhys. Lett.* **1995**, *32*, 729. (b) Kresse, G.; Furthmüller, J. *Phys. Rev. B* **1996**, *54*, 11169. (c) Kresse, G.; Furthmüller, J. *Comput. Mater. Sci.* **1996**, *6*, 15.
(28) Vanderbilt, D. *Phys. Rev. B* **1990**, *41*, 7892.
(29) (a) Alfè, D. 1998,program available at http://chianti.geol.ucl.ac.uk/~dario. (b) Alfè, D.; Price, G. D.; Gillan, M. J. *Phys. Rev. B* **2001**, *64*, 04512316.
(30) The factor group coupling for the D_{2h} point group predicts that each molecular vibration would split into eight modes. However, because the interactions between molecules are very weak, the splitting is negligible. Therefore, the frequencies listed in Table 2 are in each case the averaged values from eight modes split from one molecular vibration under the crystal field. Consequently, the symmetry assignments in Table 2 are not for the crystal symmetry group but for the C_s symmetry of a single RDX molecule.
(31) Botcher, T. R.; Wight, C. A. *J. Phys. Chem.* **1994**, *98*, 5441.
(32) Melius, C. F. In *Chemistry and Physics of Energetic Materials*; Bulusu, S. N., Ed.; Kluwer Academic Publishers: Norwell, MA, 1990; Vol. 309, p 21.
(33) Wang, J.; Brower, K. R.; Naud, D. L. *J. Org. Chem.* **1997**, *62*, 9055.
(34) Behrens, R., Jr.; Bulusu, S. *J. Phys. Chem.* **1991**, *95*, 5838.
(35) Chakraborty, D.; Muller, R. P.; Dasgupta, S.; Goddard, W. A., III. *J. Phys. Chem. A* **2000**, *104*, 2261.
(36) Zhao, X.; Hintsa, E. J.; Lee, Y. T. *J. Chem. Phys.* **1988**, *88*, 801.
(37) Habibollahzadeh, D.; Grodzicki, M.; Seminario, J. M.; Politzer, P. *J. Phys. Chem.* **1991**, *95*, 7699.

JP807285U